Mechanical, nanomorphological and biological reconstruction of early-stage apoptosis in HeLa cells induced by cytochalasin B

XUELIAN SU[1-4], LING ZHANG[3], HONG KANG[3], BAOPING ZHANG[3], GUANGJIE BAO[2,4] and JIZENG WANG[1,3]

[1]College of Civil Engineering and Mechanics, Lanzhou University, Lanzhou, Gansu 730000; [2]Key Laboratory of Stomatology of The State Ethnic Affairs Commission, Northwest Minzu University, Lanzhou, Gansu 730030; [3]Key Laboratory of Mechanics on Disaster and Environment in Western China, The Ministry of Education of China, Lanzhou University, Lanzhou, Gansu 730000; [4]Key Laboratory of Oral Diseases of Gansu Province, Northwest Minzu University, Lanzhou, Gansu 730030, P.R. China

Received May 14, 2018; Accepted November 22, 2018

DOI: 10.3892/or.2018.6921

Abstract. There is a growing interest in the fact that mechanical signals may be as important as biological signals in evaluating cell viability. To investigate the alterations in biomechanics, nanomorphology and biological apoptotic signals during early apoptosis, an apoptosis model was established for cervical cancer HeLa cells induced by cytochalasin B (CB). The cellular mechanical properties, geometry, morphology and expression of key apoptotic proteins were systematically analyzed. The findings indicated a marked decline in cellular elastic modulus and volume and a considerable increase in surface roughness occurring prior to the activation of biological apoptosis signals (such as phosphatidylserine exposure or activation of CD95/Fas). Moreover, the depolymerization of filamentous actin aggravated the intracellular crowding degree, which induced the redistribution of different-sized protein molecules and protrusions across the cell membrane arising from excluded volume interactions. Statistical analysis revealed that the disassembly of the actin cytoskeleton was negatively correlated with the cellular elastic modulus and volume, but was positively correlated with surface roughness and CD95/Fas activation. The results of the present study suggest that compared with biological signals, mechanical and geometrical reconstruction is more sensitive during apoptosis and the increase in cell surface roughness arises from the redistribution of biophysical molecules. These results contribute to our in-depth understanding of the apoptosis mechanisms of cancer cells mediated by cytochalasin B.

Correspondence to: Professor Jizeng Wang, College of Civil Engineering and Mechanics, Lanzhou University, 222 South Tianshui Road, Lanzhou, Gansu 730000, P.R. China
E-mail: jzwang@lzu.edu.cn

Key words: biomechanics, atomic force microscopy, actin cytoskeleton, cytochalasin B, apoptosis, macromolecular crowding

Introduction

Cytochalasin B (CB) is a mycogenic toxin extracted from the fungus *Phoma* sp. CB permeates through the cell membrane into the cytoplasm and binds to the 'barbed' end ('plus' end) of the filamentous actin (F-actin), while preventing the superposition of actin monomer polymerization at this site. Consequently, the polymerization of the actin cytoskeleton is impeded and its conformation is altered (1,2), ultimately affecting cell morphology and biological processes, such as cell shrinkage, mitosis and apoptosis (3). Cytochalasins are extensively used to investigate the role of the microfilament cytoskeleton in various biological processes, including cell movement, differentiation and mitosis. However, accumulating evidence indicates that cytochalasins exert potent anticancer effects and induce apoptosis in various malignant cell types (4,5). Unlike the conventional microtubule-targeted agents (6), CB is a type of microfilament-directed drug that can potentially increase the efficacy of chemotherapeutic agents by acting synergistically with them (7,8). In addition, malignant cells have a perturbed actin cytoskeleton, which makes them susceptible to preferential damage by cytochalasins. CB may induce apoptosis of various cancer cells through intrinsic or extrinsic pathways (4,9). However, there is currently no comprehensive information available regarding the biomechanics and surface topography during early apoptosis (10,11). In addition, although chemical signals have been extensively investigated to characterize cell apoptosis (12), only a limited number of studies have systematically addressed the alterations in biomechanics, cell surface topography and biological signals related to the disruption of the microfilament cytoskeleton.

Ever since apoptosis was first described by Kerr *et al* (13), numerous studies have focused on the morphology, molecular biology and underlying biological behaviors in an attempt to elucidate the subtle molecular mechanisms involved in cell

death (14,15). Researchers have long believed that apoptosis occurs when key proteins, such as initiators caspase-8 and -9, are cleaved and activated (16,17), while overlooking the alterations in biomechanics during early-stage apoptosis. Expanding knowledge and advances in research methods have enabled researchers to examine the changes in the cytoskeleton and cell elasticity. The decrease in elastic modulus was usually measured 24 h after the cells were treated (18,19). A number of studies have focused on the decline in cellular elastic modulus following drug treatment. Pelling *et al* (20) reported that the cellular elastic modulus decreases during early-stage apoptosis, and Schulze *et al* (21) observed that alterations in the actin cytoskeleton led to changes in cellular morphology and elastic modulus. These findings suggest that a certain correlation exists among disruption of the F-actin cytoskeleton, mechanical alterations and apoptosis.

F-actin is among the most important cytoskeletal components involved in maintaining the shape and mechanical properties of the cell. Alterations in F-actin organization are inevitably accompanied by changes in cellular mechanical properties (such as cell stiffness). Bio-type atomic force microscopy (AFM) is a unique technique enabling direct measurement of the mechanical properties of living cells and detection of nanostructures on the cell surface (22). Researchers have used AFM to investigate the nanoscale morphology and mechanical properties of single living cells treated with anticarcinogens (23), and the results indicated that cell stiffness is altered when cells are exposed to cytotoxic agents, such as those used for chemotherapy. The alterations in the mechanical properties of individual cells may be used as a biomarker for evaluating apoptosis (24,25). These viewpoints indicate a subtle association among the reorganization of the actin cytoskeleton, cellular mechanics and apoptosis. However, these previous studies only focused on the mechanical phenomena at 12 or even 24 h after cell treatment, and overlooked the mechanical alterations during the early stages of drug treatment. Therefore, the aim of the present study was to investigate the early alterations in biomechanics, cellular geometry, morphology and biological signals following cell exposure to CB.

For this purpose, an apoptosis model was established using HeLa cells induced by CB in order to explore the alterations and possible correlations among biomechanical reconstruction, morphological remodeling and apoptotic signal activation.

Materials and methods

Reagents and cell culture. All reagents, including CB and fluorescein isothiocyanate (FITC)-phalloidin (cat. no. P5282), were purchased from Sigma-Aldrich; Merck KGaA (Darmstadt, Germany), unless otherwise specified. Fetal bovine serum (FBS; SH30084) and BCA protein assay kit (cat. no. 23227) were purchased from Thermo Fisher Scientific, Inc. (Waltham, MA, USA). The primary anti-Fas antibody (dilution 1:200, rabbit mAb; cat. no. 133619) and primary anti-vinculin antibody (dilution 1:200, rabbit mAb; cat. no. 73412) were obtained from Abcam (Cambridge, UK). An Annexin V-fluorescein isothiocyanate (FITC)/propidium iodide (PI) kit (70-AP101-60) was obtained from Hangzhou MultiSciences Biotech Co., Ltd. (Hangzhou, China). Nitrocellulose membranes and cell membrane protein extraction kit (P0033) were acquired from Beyotime Institute of Biotechnology (Shanghai, China). CB (cat. no. C6762) was dissolved in dimethyl sulfoxide (D2650). The secondary antibodies Texas red fluorescent-conjugated goat anti-rabbit IgG (dilution 1:200; cat. no. 6904-250), horseradish peroxidase-labeled goat anti-rabbit IgG (dilution 1:200; cat. no. 6403-05), FITC fluorescent-conjugated IgG (dilution 1:200; cat. no. 6401-05) were obtained from BioVision, Inc. (San Francisco, CA, USA).

Human cervical cancer HeLa cells were obtained from the Cell Bank of the Chinese Academy of Sciences (Shanghai, China) and cultured in Dulbecco's modified Eagle's medium (DMEM; HyClone; GE Healthcare, Chicago, IL, USA) supplemented with 10% FBS, 100 μg/ml streptomycin and 100 U/ml penicillin in a humidified atmosphere of 5% CO_2 at 37˚C.

Fluorescence staining and F-actin visualization. To visualize the F-actin organization, cells treated with CB were stained with fluorochrome. The cell-climbing pieces (sterile coverslips preplaced in a Petri dish) were treated with 5 μg/ml CB for different time periods, rinsed with phosphate-buffered saline (PBS; pH 7.4), fixed with 4.0% cooled paraformaldehyde, permeated with 0.2% Triton X-100 in PBS, blocked with 2% bovine serum albumin (BSA; 9048-46-8; Beijing Solarbio Science & Technology Co., Ltd., Beijing, China) in PBS, and incubated with FITC fluorescent-conjugated phalloidin for 1 h at room temperature in the dark. The nuclei were labeled with 4,6-diamidino-2-phenylindole (DAPI, D9542; Sigma-Aldrich; Merck KGaA) at a concentration of 0.1 mg/ml. The coverslips were sealed on the glass slides with Antifade Mounting Medium (Beijing Solarbio Science & Technology Co., Ltd.). The specimens were observed and imaged by an Olympus FV1000 laser scanning confocal microscope (LSCM; Olympus Corp., Tokyo, Japan) in 1 week. The mean fluorescence intensity of F-actin was analyzed with FV10-ASW 4.1 Viewer software (Olympus Corp.). No other filtering or adjustments were applied.

Western blot analysis and death receptor CD95/Fas expression. Vinculin, a ubiquitously expressed actin-binding protein (ABP), can affect cell adhesion and signal transmission. To investigate whether vinculin expression was inhibited by CB, its expression was analyzed by western blotting. Samples were collected by trypsinization (~1x10^7 cells). The cell membrane protein extraction kit was used to extract the total proteins of the cell membrane. The total protein contents of the lysates were determined with the BCA protein assay kit. The proteins (30 g/well) were separated by 10% sodium dodecyl sulfate-polyacrylamide gel electrophoresis (SDS-PAGE) and then transferred onto nitrocellulose membranes. Non-specific proteins were blocked with 5% skimmed milk powder diluted in Tris-buffered saline containing 0.05% Tween-20 at room temperature for 1 h. Then, primary anti-vinculin antibodies (1:1,000 dilution) and anti-GAPDH antibodies (1:1,000 dilution; cat. no. 22555; Abcam) were added and incubated at 4˚C overnight. The blots were incubated with horseradish peroxidase-labeled goat anti-rabbit secondary antibodies at room temperature for 1 h. The bands were exposed by a Tanon-5200 imaging system (Tanon Science and Technology Co., Ltd., Shanghai, China), and the intensity was quantified

using the ImageJ 2x software [National Institutes of Health (NIH) Bethesda, MD, USA].

After treatment, the cell-climbing pieces were fixed, permeated and incubated with rabbit monoclonal primary anti-Fas antibodies (1:200 dilution) at 4˚C overnight, colored with Texas Red fluorescent-conjugated secondary antibodies, then incubated with rabbit polyclonal anti-vinculin antibodies (1:200 dilution) at 37˚C for 2 h, and colored with FITC fluorescent-conjugated secondary antibodies. The nuclei were labeled with DAPI. All procedures were performed in the dark. The specimens were observed and imaged using LSCM.

Annexin V-FITC/PI apoptotic analysis. During apoptosis, phosphatidylserine (PS) translocates to the membrane surface. Acting as an 'eat me' signal, PS exposure prompts phagocytes to engulf apoptotic cells (26), which is a relatively late stage of the apoptosis process. PS externalization is common in early apoptosis (27). A recent study demonstrated that PS exposure in response to apoptotic stimuli is mediated by the phospholipid scramblase Xkr8, which is activated directly by caspases. But the authors also pointed out that this effect is only observed in the late stages of apoptosis (28). In addition, in early apoptosis, the intracellular Ca^{2+} concentration increases, which mediates PS exposure. Accordingly, the present study used PS exposure to determine the occurrence of apoptosis, and then designed subsequent experiments. Annexin V has a high affinity for PS. Thus, PS translocation was analyzed by flow cytometry (FCM) using an Annexin V-FITC/PI apoptosis detection kit, in accordance with the manufacturer's instructions. The cells ($5x10^5$) were loaded onto a 60-mm Petri dish, incubated overnight, treated with 5 μg/ml CB, and collected by trypsinization. Then, the cell pellets were resuspended in 100 μl binding buffer, followed by staining with 5 μl Annexin V-FITC and 5 μl PI for 30 min at room temperature in the dark. All the samples were analyzed with a FACSCalibur flow cytometer (BD Biosciences, Franklin Lakes, NJ, USA) and the data were evaluated using the CellQuest software (BD Biosciences).

AFM imaging and nanoindentation mechanical analysis. A commercial NanoWizard III AFM (JPK Instruments, Berlin, Germany) was utilized for cell imaging and probing the force spectroscopy of living HeLa cells. This microscope was combined with an inverted optical microscope (Carl Zeiss AG, Oberkochen, Germany) to facilitate AFM and optical microscopy imaging simultaneously. Silicon nitride cantilevers (PNP-DB; NanoWorld AG, Neuchatel, Switzerland) with a nominal spring constant of 0.03 N/m (f_o: 17 kHz) were used in all experiments. AFM images and force spectroscopy measurements were collected under intermittent mode by using a square pyramidal silicon nitride probe with a 4.0-nm tip diameter and a 25˚C half-opening angle. Prior to the AFM measurements, the sensitivity and the spring constants of the cantilevers were calibrated using JPK Instruments 4.2.61 software. A square pyramidal tip with a spring constant of 0.029 N/m was used in the subsequent experiments. The inverted optical microscope was used to select the ideal cell and position of the AFM tip. All AFM images and nanoindentation experiments were conducted in cell culture medium at room temperature according to previously described operating procedures (29,30). The AFM had a scanning range of 80x80 μm (x- and y-axes) and a vertical range (z-axis) of 15 μm. The cells were imaged at 512x512 pixels. Then, 10-15 dots around the nucleus (orange area) were selected to obtain the force-distance curves from the indentation of the living cells. The interaction between the tip and sample caused a cantilever deflection, which was recorded as a function of the relative sample position, i.e., a force-distance curve. The elastic modulus (cell stiffness) was calculated by using JPK Instruments data processing 4.2.61 software to analyze 130-160 approach curves of force spectroscopy.

Cell height, roughness and volume measurement. The height of the cell, which was defined as the distance between the top and bottom, was determined from the height-measured images. The height, diameter and average roughness of each cell were measured by cross-sectional analysis. Average roughness (Ra) and root mean square (RMS) roughness (Rq) are key surface roughness parameters for understanding the nanoscale surface morphology of cells. The analysis of the surface roughness provides novel quantitative data on cell nanomorphology. The cellular volume is another important indicator for understanding the state of the cell. If the cell is considered as the half of an oblate ellipsoid, then the cell volume can be calculated as follows (31):

$$V = \frac{2}{3}\pi r^2 h$$

where V is the volume, r is the radius and h is the height of the cell.

Mechanical property measurement. AFM is an effective tool for assessing the mechanical properties of single living cells via nanoindentation tests under physiological conditions (24,25). If the cell is considered as an elastomer of homogeneous structure, the cell elastic modulus E is calculated according to the Hertz model and the approach curves (32,33). The indentation depth (5-10% of the height of the cell, ~200-500 nm) is fitted using JPK Data Processing software (JPK Instruments) (34,35). The referential equation indicating the relation between indentation force and depth is as follows:

$$F = \delta^2 \frac{2}{\pi} \frac{E}{1-\mu^2} \tan\theta$$

where F is the loading force, E is the elastic modulus, δ is the indentation depth, μ is the Poisson's ratio of the samples, and θ is the half-opening angle of the pyramidal tip.

Cell surface visualization by scanning electron microscopy. The spinous protrusions and surface morphological changes at the nanoscale level were observed by CLSM and AFM after the cells were treated with CB at different time-points. To further elucidate these phenomena, we created specimens for scanning electron microscopy (SEM) and observed the cell surface. The cells were seeded ($5x10^3$ cells) onto a 24-well plate (preplaced sterile coverslips), cultivated for 48 h, and treated with 5 μg/ml CB for 0, 0.5 and 3 h. The samples were rinsed with cold PBS, fixed with 3% pre-cooled glutaraldehyde solution at 4˚C overnight, and made into ultra-thin slices. The cell surface morphology was observed and captured by

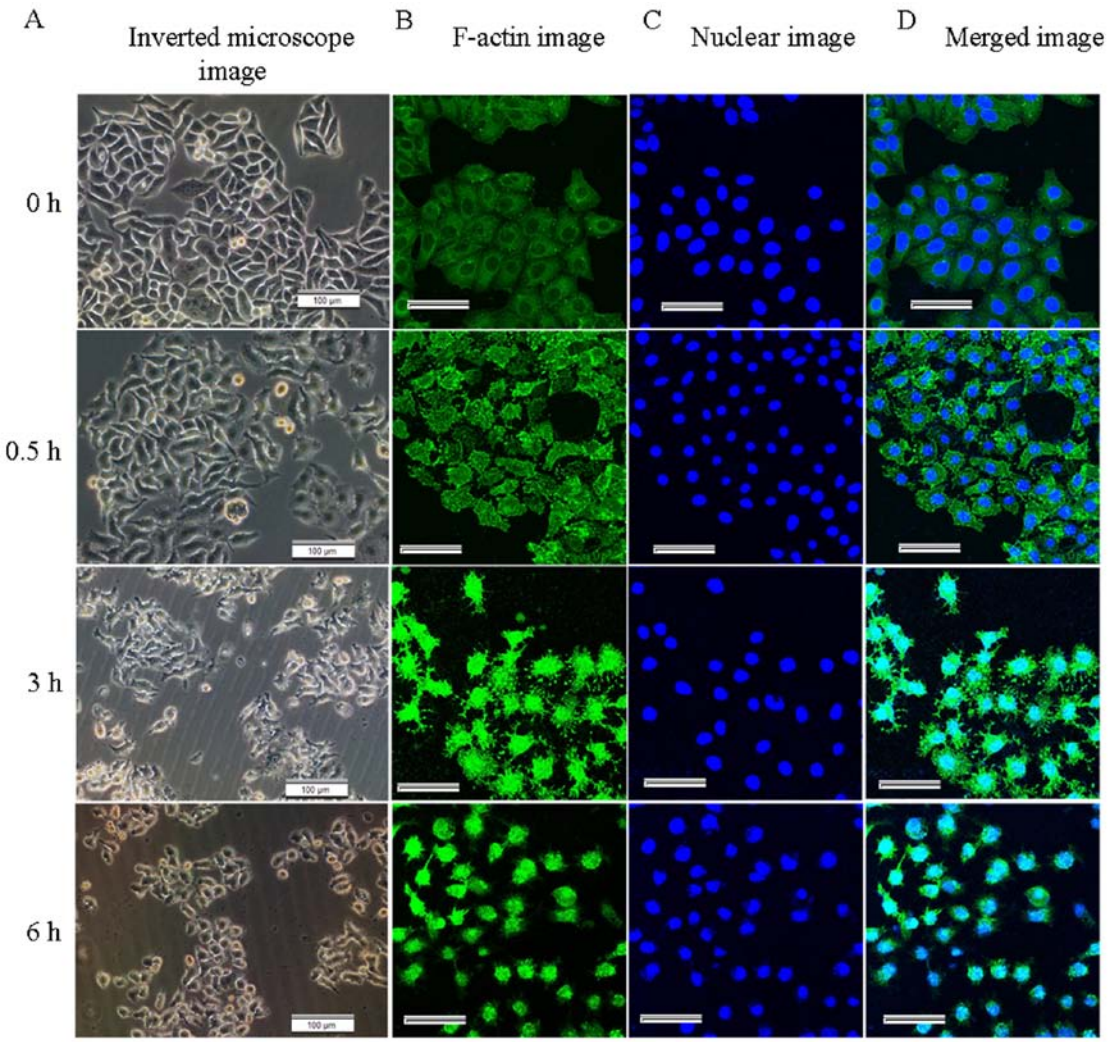

Figure 1. Effect of cytochalasin B (CB) on cell morphology and the F-actin cytoskeleton at different time-points. (A) Optical micrographs. Scale bars, 100 μm. Untreated cells exhibited normal morphology, while the CB-treated cells gradually shrank, rounded up, even became detached from the substrate and floated. (B) In addition, F-actin was disrupted in the treated cells, and the short or punctate actin fragments (green fluorescence) occupied the background of the images. (C) The nucleus (blue fluorescence) appeared irregular at 6 h. (D) Merged images. Scale bars, 50 μm.

using a scanning electron microscope (JSM6380 LV; JEOL, Ltd., Tokyo, Japan).

Statistical analysis. Data are recorded as mean ± standard deviation and analyzed using SPSS 22.0 (Statistical Product and Service Solutions; IBM Corp. Armonk, NY, USA). Statistical comparisons were performed using one-way analysis of variance ANOVA followed with Dunnett's t-tests. $P<0.05$ or $P<0.01$ were considered to indicate statistically significant differences. Single asterisks (*) indicate a significant difference ($P<0.05$), and double asterisks (**) denote an extremely significant difference ($P<0.01$).

Results

Morphological changes and actin cytoskeletal depolymerization. The morphological changes of the HeLa cells treated with CB were observed using an Olympus CKX31 inverted microscope (Olympus Corp.). The untreated cells were well-spread and the cell borders were clear. By contrast, the CB-treated cells gradually shrank, rounded up, even became detached from the substrate and floated (Fig. 1A). The fluorescent-labelled F-actin and nucleus were observed by LSCM. In the control groups, the F-actin was uniformly distributed beneath the cell membrane around the nuclei. In the treated groups, the F-actin was disrupted, with short or punctate actin fragments (green fluorescence) occupied the background of the images. Numerous spinous protrusions appeared at the periphery of the cells, particularly at 3 h (Fig. 1B). These changes indicated that filamentous actin was gradually depolymerized and disrupted by CB. As the disruption of the actin cytoskeleton progressed, the adherent area of the cells gradually decreased and the nucleus became irregular at 6 h (Fig. 1C). The fluorescence intensity of F-actin gradually increased, reaching its maximum at 2 h, and then gradually decreased (Fig. 2D), further reflecting the disruption of the actin cytoskeleton, and the density of the intracellular actin fragments increased.

Effect of cytochalasin B on PS exposure. Annexin V-FITC/PI apoptosis analysis revealed that the apoptosis marker PS was almost undetectable during the initial 3 h (Fig. 2A-C). Then,

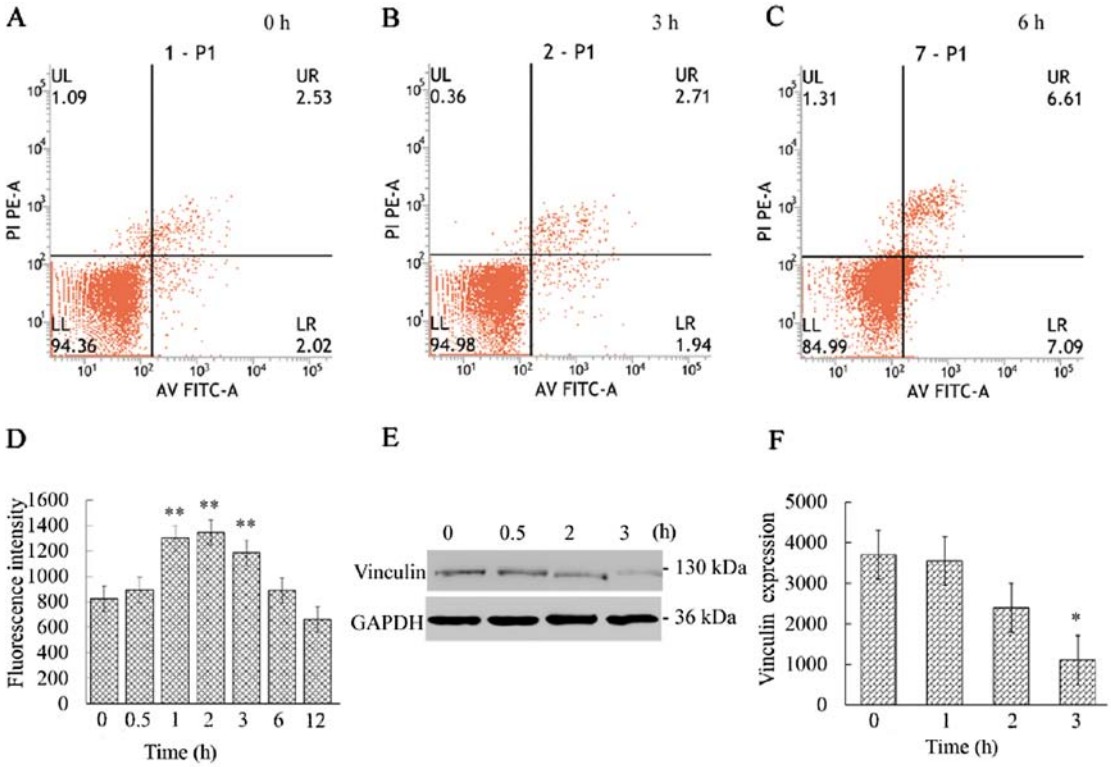

Figure 2. Apoptosis, fluorescence intensity of F-actin and vinculin expression analysis. (A-C) Phosphatidylserine (PS) were almost undetectable during the initial 3 h and were measurable at 6 h. (D) The fluorescence intensity of F-actin was significantly increased, reaching its maximum at 2 h ($P<0.01$). (E and F) Vinculin expression continuously decreased and was found to be significantly reduced at 3 h ($P<0.05$). The results are presented as mean ± standard deviation and were analyzed by one-way analysis of variance (ANOVA). $^{*}P<0.05$ and $^{**}P<0.01$.

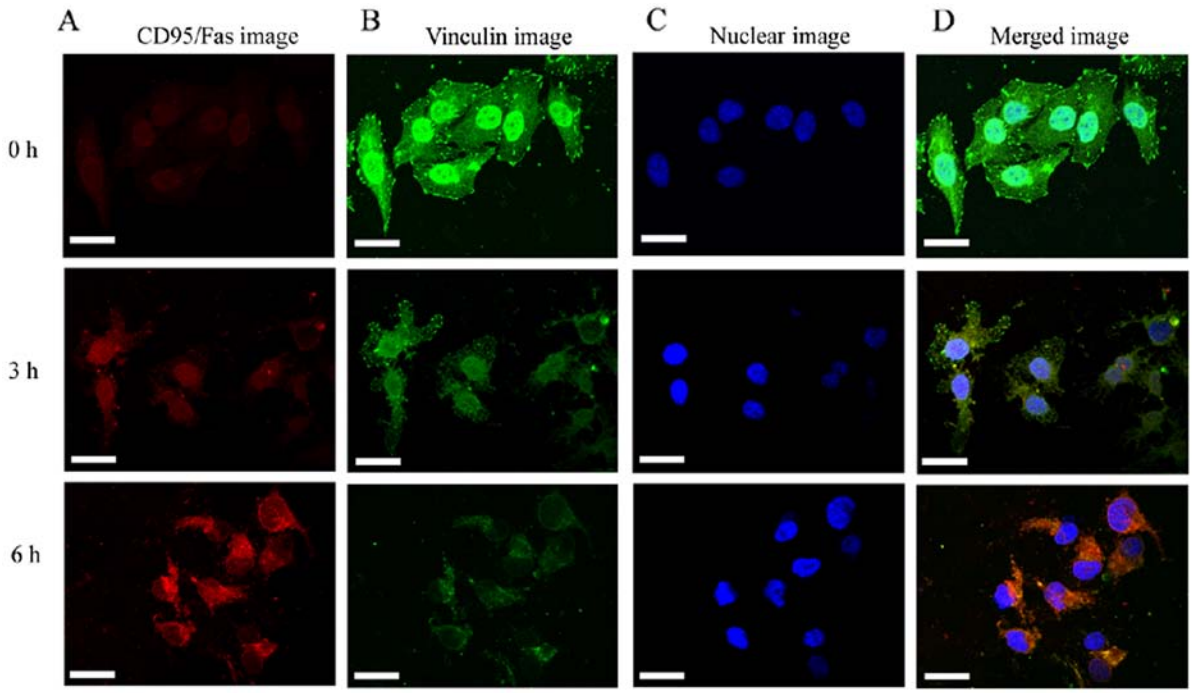

Figure 3. Immunofluorescence staining of HeLa cells death receptor CD95/Fas and vinculin protein under treatment with cytochalasin B. (A and D) Only a mild activation of CD95/Fas was observed, indicated by weak red fluorescence at 3 h, whereas the red fluorescence was considerably brighter at 6 h. (B and D) By contrast, in untreated cells, the vinculin staining exhibited bright dot green fluorescence, whereas in the treated cells it was continuously diminished, with only a small amount of green fluorescence surrounding the nucleus at 6 h. (C) The nucleus (blue fluorescence) appeared irregular at 6 h. Scale bars, 20 μm.

the apoptosis rate gradually increased, reaching 14.77% at 12 h (data not shown).

The aforementioned results demonstrate that the actin cytoskeleton was markedly disrupted after the cells were

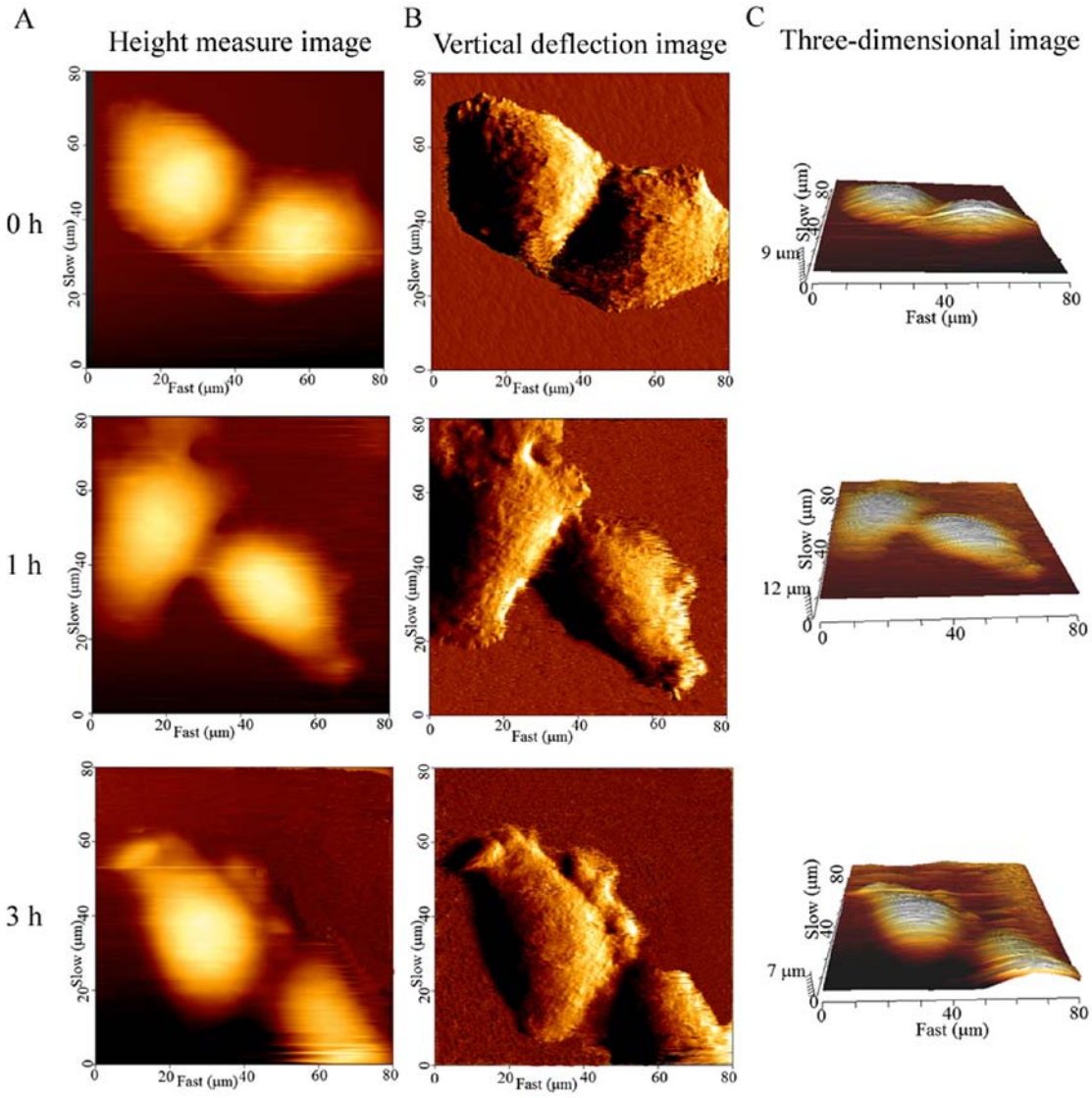

Figure 4. Cell surface topography captured by atomic force microscopy at different time-points. (A-C) Height-measured, vertical deflection and three-dimensional images, respectively, at a scan scale of 80x80 μm are shown. The boundaries of the untreated cells are clear; however, the peripheries of treated cells became irregular and protrusions appeared.

treated with CB. The FCM analysis revealed that obvious apoptosis was almost not detected during the initial 3 h and the disruption of the F-actin cytoskeleton occurred prior to PS exposure on the cell surface. This phenomenon indicates that CB mediates apoptosis through targeting the actin cytoskeleton.

Downregulation of vinculin and activation of CD95/Fas. The vinculin expression was continuously decreased and was found to be significantly ($P<0.05$) reduced at 3 h (Fig. 2E and F). The results indicated that the destruction of the actin cytoskeleton resulted in the reduction of vinculin expression, which destroyed the signaling pathway that connects internal and external signal transmission. The decrease in vinculin expression is likely the cause of the activation of the cell membrane death receptor CD95/Fas. Several studies have demonstrated that apoptosis was accompanied by decreased vinculin expression and the activation of CD95/Fas (4,36). These findings are consistent with our results that the CD95/Fas (red fluorescence) was mildly activated at 3 h and significantly activated at 6 h, whereas the vinculin expression (green fluorescence) gradually decreased (Fig. 3).

Geometric reconstruction and surface roughness increase. The cellular height, diameter and roughness were measured by the cross-sectional analysis of the height-measured images (Fig. 4A-C). Ra and Rq are key parameters for understanding the cellular surface topography at the nanoscale level. The cell surface roughness differed significantly before and after the cells were exposed to CB, and this change occurred in a time-dependent manner. The control cells displayed the smallest Ra (0.97±0.09 mm) and Rq (1.12±0.12 mm), while the average Ra and Rq of the treated cells were significantly higher ($P<0.01$) than that of the control (Fig. 5A and B). These findings were consistent with the spinous protrusions at the periphery of cells, as observed by LSCM. However, the cause of the increased cell surface roughness remains unknown. Thus, the cell surface was then observed by SEM.

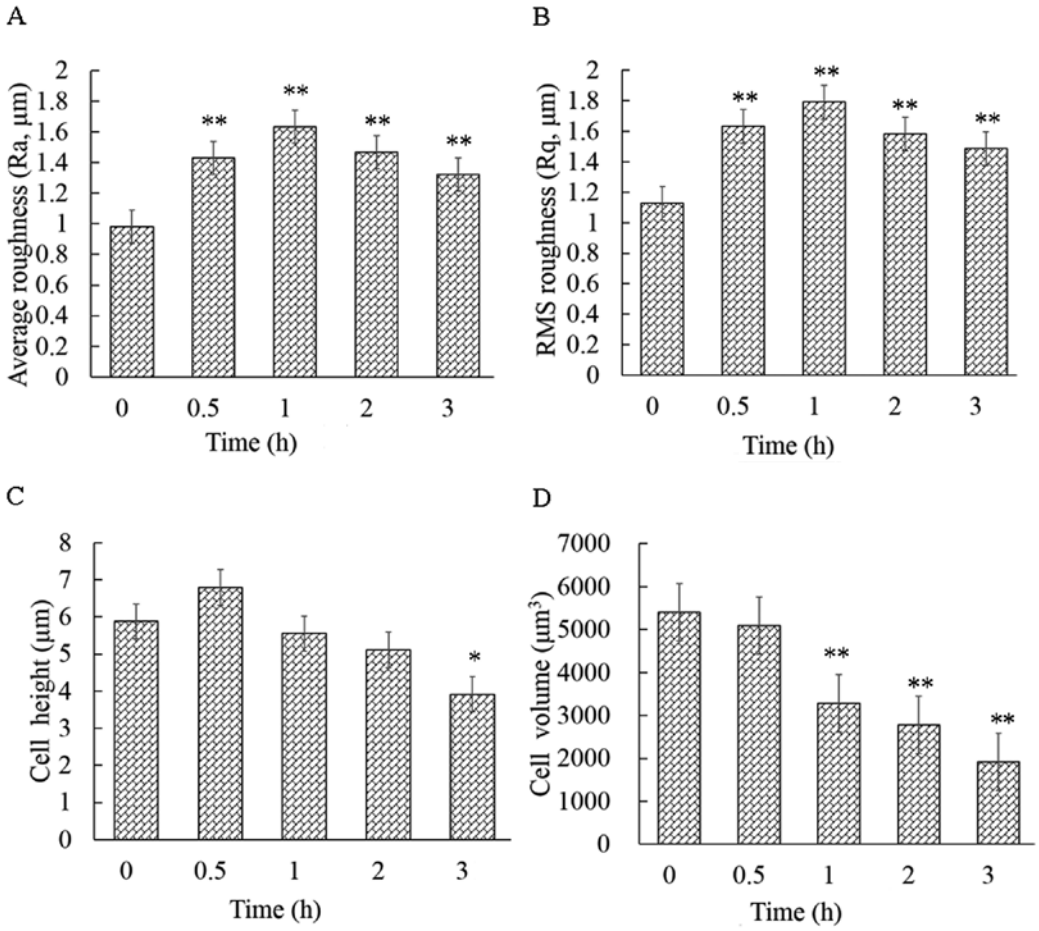

Figure 5. Effects of cytochalasin B (CB) on surface roughness and geometry of HeLa cells. (A and B) The surface roughness parameters Ra and Rq increased significantly following treatment of the cells with CB, and reached their maximum value at ~1 h (P<0.01). (C) The cell height changed drastically, increasing at 0.5 h of exposure and subsequently decreasing. (D) The cell volume continuously declined (P<0.01). The results are presented as the mean ± standard deviation and were analyzed by one-way analysis of variance (ANOVA). *P<0.05 and **P<0.01. Ra, average roughness; Rq, root mean square (RMS) roughness.

In addition, the CB-induced apoptosis was accompanied by a decrease in volume. The brightly colored area was at the highest part of the cell on the height-measured images (Fig. 4A). The mean cellular height changed drastically, increasing at 30 min of exposure and subsequently decreasing (Fig. 5C). However, the cellular mean volume changed continuously, decreasing from 5,404±752 to 1,919±506 μm^3 in 3 h (Fig. 5D). In particular, the volume significantly declined (P<0.01) with respect to the control within 1 h of exposure.

Decrease in the elastic modulus of HeLa cells. After the cell height image was captured, 10-15 dots were selected around the nucleus to perform the nanoindentation experiment (Fig. 6A) and obtain the force-distance curves (Fig. 6B-E). The red and blue lines denote the extend curves and the retract curves, respectively. The elastic modulus *E* was normally distributed. Most of the *E* values were concentrated around the mean *E* value of each group and the mean *E* was 5.84±0.88 MPa for the control. After the cells were exposed to CB, *E* significantly decreased (P<0.01) to 1.30±0.33 MPa at 3 h (Fig. 6F), suggesting that the cells became increasingly softer as F-actin was damaged during the treatment.

The elastic modulus is mainly determined by the F-actin component of the cytoskeleton. The mechanical properties are also recognized as indicators of physiological processes, such as malignant phenotype, differentiation and mitosis. In the present experiment, the cellular elastic modulus significantly declined within 3 h. However, PS, which is an early biological apoptosis marker, remained undetectable at that time. Therefore, the elastic modulus had obviously decreased before biological signals were detected, indicating that the cellular mechanical reconstruction preceded the biological alterations during CB-induced apoptosis.

Ultrastructural changes in HeLa cells. The surface of the control cells was smooth, with only a few tiny points observed (Fig. 7A and D). Microvilli, lamellipodia and filopodia were identifiable. By contrast, the surface of the treated cells became considerably rough, with numerous filaments passing through the membrane and located on cell surface (Fig. 7B and C, E and F). Actin fluorescence staining also revealed a large number of filamentous structures at the periphery of the cells (Fig. 7H) while these structures were not seen around the cells of the control (Fig. 7G). This phenomenon may be the reason for the rougher surface observed during the treatment. However, only the filaments passing through the membrane could be seen, as we were unable to determine whether these filaments were the F-actin fragments disrupted by CB.

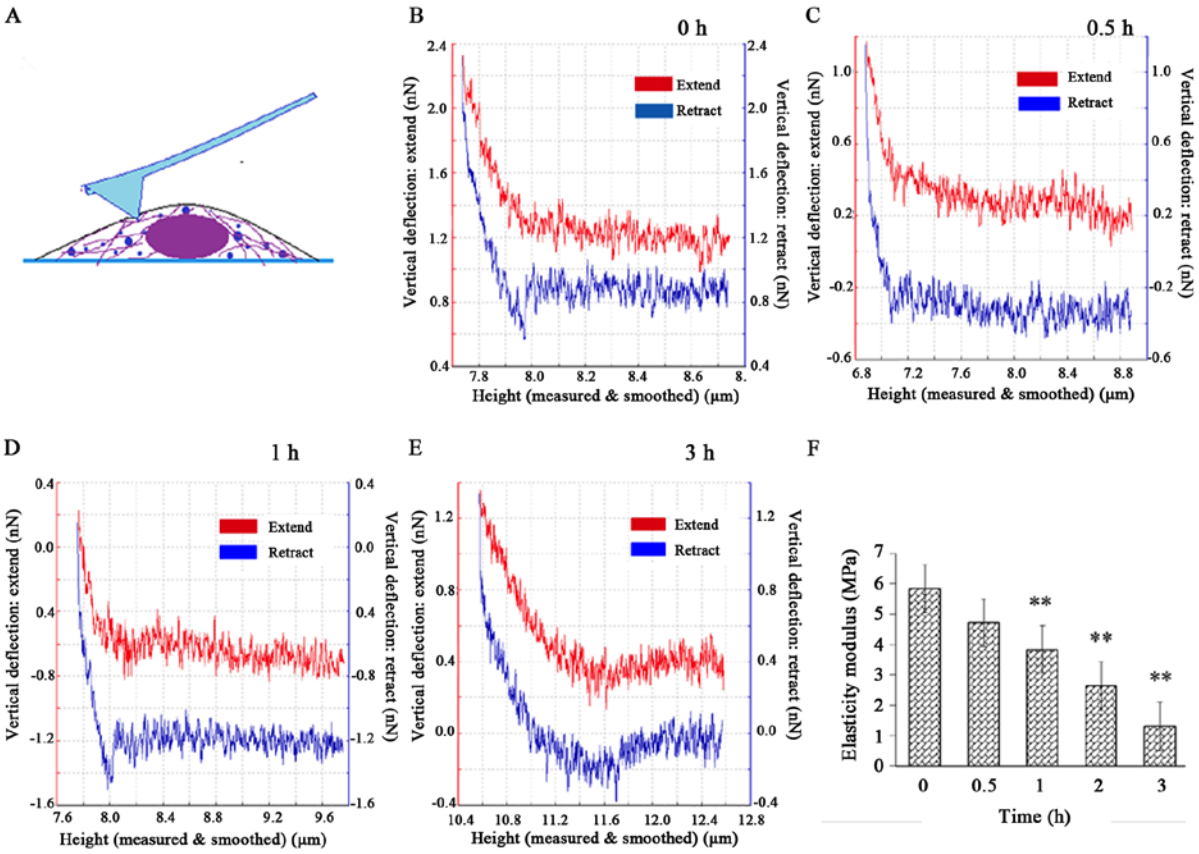

Figure 6. Nanoindentation experiment on HeLa cells and analysis of results. Schematic diagram of the nanoindentation experiment: (A) The indentation points were selected in the cytoplasmic region around the nucleus. (B-E) The force-distance curves were obtained by nanoindentation with atomic force microscopy. The red lines denote the extend curves, and the blue lines represent the retract curves. (F) The elastic modulus of the cells gradually decreased, with a statistically significant difference at 1 h ($P<0.01$). The results are presented as the mean ± standard deviation and were analyzed by one-way analysis of variance. $^{**}P<0.01$.

Discussion

In the present study, the alterations in biomechanics, geometry and biological signals were systematically investigated during cytochalasin B (CB)-triggered HeLa cell apoptosis. The findings demonstrated that the destruction of F-actin rapidly led to a decrease in the elastic modulus and volume of the cells, and an increase in the cell surface roughness and intracellular crowding, followed by gradual exposure of PS on the plasma membrane and activation of the cell membrane death receptor CD95/Fas. Previous studies by our research group have found that there are coupling interplays between biological apoptotic signals and biomechanical remodeling during apoptosis (28). Therefore, further studies on alterations in biomechanics contribute to a better understanding of the anticancer mechanism of action of actin-targeted drugs, such as cytochalasins.

Apoptosis is a complex multi-step process involving a series of biological signals. Its characterization includes morphological changes (cell contraction, chromatin condensation, nuclear fragmentation and cytoplasmic membrane blebbing) and energy-dependent biochemical molecular event cascades (PS exposure, caspase activation and protein cross-linking) (37). However, with the improvements in research methods and the continuous elucidation of apoptosis, a growing number of studies report that apoptosis is not only a cascade of biochemical signals, but is also accompanied by cellular mechanical remodeling. In the present study, it was found that the biological apoptotic marker PS did not expose on the cell surface, CD95/Fas clustering was not obvious within the first 3 h of CB treatment. But the elastic modulus and volume of the cells were significantly decreased, and the surface roughness was significantly increased. This finding is consistent with the results of a recent study (38), supporting that the significant changes in mechanical activity were measured while the alterations in biological activity were yet undetected. These significant changes in cellular mechanics may be measured due to the superiority of the means of mechanical research. The AFM adopted in the present study does not require complex cellular processing and directly detects the mechanical behavior of cells at the nanometer level under physiological conditions in a real-time, quantitative and free-labeled manner. Therefore: i) compared with biological signals, mechanical and geometrical reconstruction is more sensitive during apoptosis; and ii) compared with biological technology, biomechanical technology is more sensitive for the detection of apoptosis.

HeLa cells induced by CB were observed by SEM, and it was found that the lamellipodia and filopodia contracted, and a large number of filamentous structures appeared on the cell surface at 30 min. These filamentous structures were denser at 3 h. Actin fluorescence staining also revealed a large number of spiny structures at the periphery of the

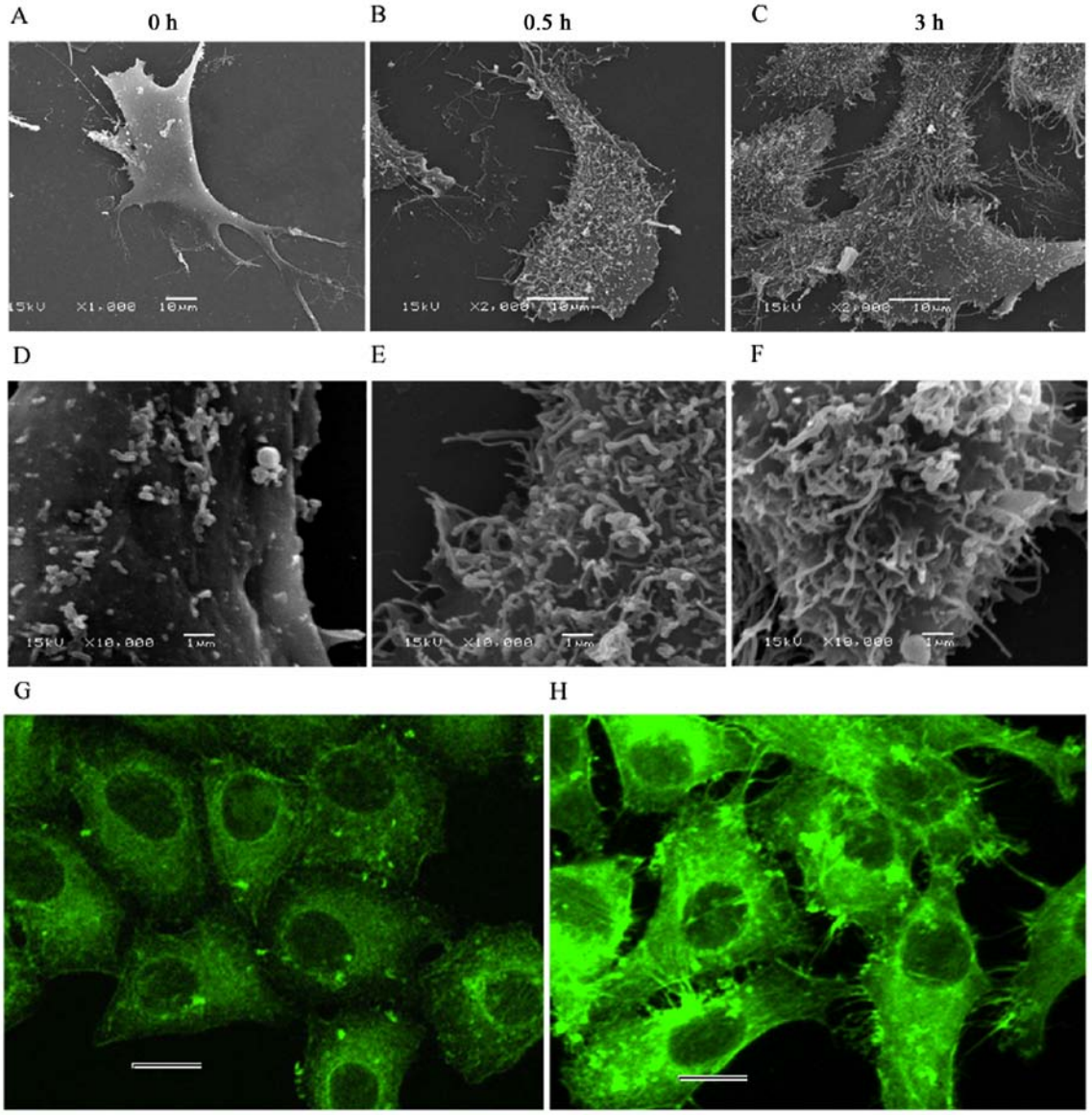

Figure 7. Ultrastructure of HeLa cells observed by scanning electron microscopy and F-actin fluorescent staining. Overall views of the cell at (A-C) low magnification; and (D-F) partially enlarged views at high magnification. (A and D) Normal characteristics were observed for microvilli, lamellipodia and filopodia in control cells. (B and C, E and F) By contrast, the surface appeared considerably rough with numerous filamentous structures on the surface of the treated cells. (G) F-actin was uniformly distributed, while (H) numerous green fluorescent filaments appeared at the periphery of the CB-treated cells. Scale bars, 20 μm.

cells (Fig. 7H). According to the apoptotic morphological characteristics, cytoplasmic membrane blebbing appears during apoptosis (39). The morphological features of the cell surface upon cytochalasin B treatment largely resemble the well-documented cytoplasmic membrane blebbing during apoptosis, which is mediated by caspase-triggered activation of the Rho effector ROCK I b promoting myosin light chain protein phosphorylation (40). Therefore, it is possible that mechanical and geometrical features induced by cytochalasin B could be the results of biological signals of apoptotic cells, such as activation of apoptosis-specific nucleases and proteases. However, the ultrastructure of HeLa cells after treatment with *Polyalthia longifolia* leaf extract (PLME) was observed by SEM, and membrane blebbing appeared at ~12 h (41). This finding is roughly consistent with the significant activation of caspase at ~16-24 h during CB-mediated HeLa cell apoptosis (4,9). However, the increased surface roughness was observed within 3 h after the HeLa cells were treated with CB (its effect is equivalent to that of PLME). Moreover, the filamentous structures were completely different from the blebbing described in the literature (41). CB induces apoptosis by disruption of the actin cytoskeleton and the fragments of actin aggravated intracellular crowding. As a matter of fact, eukaryotic cells are surprisingly crowded (42). According to Monte Carlo simulations (43), the increase in molecular crowding leads to biophysical molecule redistribution. In semi-permeable biofilm cavity, as the crowding increases, the macromolecules are redistributed to the wall of the cavity, allowing some molecules to protrude across the biofilm (44). The protrusions are the filamentous structures observed by SEM and are also responsible for the increased cell surface roughness. Taken together, these findings suggest that the changes in cell surface roughness are caused by the redistribution of protein molecules inside the cells.

In addition to the changes in mechanics, geometry and surface roughness, cytoskeletal disruption was accompanied by the downregulation of vinculin expression. Vinculin, a widely expressed ABP, connects the actin cytoskeleton and the focal adhesion proteins and is involved in the formation of the focal adhesion-actin cytoskeleton signaling cascade (45). Vinculin can affect this cascade and modulate cell survival and apoptosis through focal adhesion proteins. For example, vinculin regulates apoptosis by disturbing the interactions between focal adhesive kinase (FAK) and paxillin (46). Interfering with FAK can induce the activation of CD95/Fas-related death domains, leading to apoptosis (47). The present study only found that vinculin expression continuously decreased and the CD95/Fas was gradually activated during apoptosis. The downregulation of vinculin disrupted the focal adhesion-cytoskeletal signaling cascade. However, there is not any evidence to support a direct cause-effect relationship between the vinculin expression and CD95/Fas activation. Vinculin expression decrease was only correlated with the increase in CD95/Fas expression.

The CB-triggered disruption of the actin cytoskeleton rapidly caused the decrease in cellular elasticity and volume, and the increase in cell surface roughness and intracellular crowding, ultimately leading to apoptosis. Moreover, these alterations occurred prior to the changes of biological apoptosis signals, including PS and CD95/Fas.

In summary, the results of the present study suggested that, compared with biological signals, biomechanical and geometric reconstruction is more sensitive during apoptosis. The CB-induced disruption of the actin cytoskeleton causes redistribution of protein molecules inside the cells, and some protein molecules protrude from the cell membrane, which is an explanation for the observed increased cell surface roughness. These findings may improve our understanding of the apoptosis mechanisms of cancer cells mediated by cytochalasins.

Acknowledgements

The authors thank the Key Lab of Stomatology of State Ethnic Affairs Commission (Northwest Minzu University) and Ms. Fei Tang and Mr. Ming-zhong Chen for their technical assistance with the flow cytometric analysis and imaging with CLSM, respectively.

Funding

The present study was supported by grants from the Fundamental Research Funds for the Central Universities (no. 31920150006, lzujbky-2017-ot11) and the National Nature Science Foundation of China (nos. 11472119, 11421062 and 81660189).

Availability of data and materials

The datasets used during the present study are available from the corresponding authors upon reasonable request.

Authors' contributions

XS performed most of the experiments. JW and HK designed the experiments and coordinated the project. GB, BZ and LZ participated in the *in vitro* study. All authors participated in the collection of the data. All authors read and approved the manuscript and agree to be accountable for all aspects of the research in ensuring that the accuracy or integrity of any part of the work are appropriately investigated and resolved.

Ethics approval and consent to participate

Not applicable.

Patient consent for publication

Not applicable.

Competing interests

The authors declare that they have no conflict of interest.

References

1. Bonder EM and Mooseker MS: Cytochalasin B slows but does not prevent monomer addition at the barbed end of the actin filament. J Cell Biol 102: 282-288, 1986.
2. Zigmond SH: Beginning and ending an actin filament: Control at the barbed end. Curr Top Dev Biol 63: 145-188, 2004.
3. Gourlay CW and Ayscough KR: The actin cytoskeleton: A key regulator of apoptosis and ageing? Nat Rev Mol Cell Biol 6: 583-589, 2005.
4. Kulms D, Düssmann H, Pöppelmann B, Ständer S, Schwarz A and Schwarz T: Apoptosis induced by disruption of the actin cytoskeleton is mediated via activation of CD95 (Fas/APO-1). Cell Death Differ 9: 598-608, 2002.
5. Trendowski M, Christen T, Acquafondata C and Fondy T: Effects of cytochalasin congeners, microtubule-directed agents, and doxorubicin alone or in combination against human ovarian carcinoma cell lines in vitro. BMC Cancer 15: 632, 2015.
6. Walker SR, Chaudhury M, Nelson EA and Frank DA: Microtubule-targeted chemotherapeutic agents inhibit signal transducer and activator of transcription 3 (STAT3) signaling. Mol Pharmacol 78: 903-908, 2010.
7. Bezabeh T, Mowat MR, Jarolim L, Greenberg AH and Smith IC: Detection of drug-induced apoptosis and necrosis in human cervical carcinoma cells using 1H NMR spectroscopy. Cell Death Differ 8: 219-224, 2001.
8. Raguz S and Yagüe E: Resistance to chemotherapy: New treatments and novel insights into an old problem. Br J Cancer 99: 387-391, 2008.
9. Hwang J, Yi M, Zhang X, Xu Y, Jung JH and Kim DK: Cytochalasin B induces apoptosis through the mitochondrial apoptotic pathway in HeLa human cervical carcinoma cells. Oncol Rep 30: 1929-1935, 2013.
10. Lecuit T and Lenne PF: Cell surface mechanics and the control of cell shape, tissue patterns and morphogenesis. Nat Rev Mol Cell Biol 8: 633-644, 2007.
11. DuFort CC, Paszek MJ and Weaver VM: Balancing forces: Architectural control of mechanotransduction. Nat Rev Mol Cell Biol 12: 308-319, 2011.
12. Bakal C, Aach J, Church G and Perrimon N: Quantitative morphological signatures define local signaling networks regulating cell morphology. Science 316: 1753-1756, 2007.
13. Kerr JF, Wyllie AH and Currie AR: Apoptosis: A basic biological phenomenon with wide-ranging implications in tissue kinetics. Br J Cancer 26: 239-257, 1972.
14. Qiu M, Chen L, Tan G, Ke L, Zhang S, Chen H and Liu J: A reactive oxygen species activation mechanism contributes to JS-K-induced apoptosis in human bladder cancer cells. Sci Rep 5: 15104, 2015.
15. Fulda S: Molecular pathways: Targeting inhibitor of apoptosis proteins in cancer-from molecular mechanism to therapeutic application. Clin Cancer Res 20: 289-295, 2014.
16. Li J and Yuan J: Caspases in apoptosis and beyond. Oncogene 27: 6194-6206, 2008.

17. Jeong JJ, Park N, Kwon YJ, Ye DJ, Moon A and Chun YJ: Role of annexin A5 in cisplatin-induced toxicity in renal cells: Molecular mechanism of apoptosis. J Biol Chem 289: 2469-2481, 2014.
18. Kim KS, Cho CH, Park EK, Jung MH, Yoon KS and Park HK: AFM-detected apoptotic changes in morphology and biophysical property caused by paclitaxel in Ishikawa and HeLa cells. PLoS One 7: e30066, 2012.
19. Susanto O, Stewart SE, Voskoboinik I, Brasacchio D, Hagn M, Ellis S, Asquith S, Sedelies KA, Bird PI, Waterhouse NJ, *et al*: Mouse granzyme A induces a novel death with writhing morphology that is mechanistically distinct from granzyme B-induced apoptosis. Cell Death Differ 20: 1183-1193, 2013.
20. Pelling AE, Veraitch FS, Chu CP, Mason C and Horton MA: Mechanical dynamics of single cells during early apoptosis. Cell Motil Cytoskeleton 66: 409-422, 2009.
21. Schulze C, Müller K, Käs JA and Gerdelmann JC: Compaction of cell shape occurs before decrease of elasticity in CHO-K1 cells treated with actin cytoskeleton disrupting drug cytochalasin D. Cell Motil Cytoskeleton 66: 193-201, 2009.
22. Müller DJ and Dufrêne YF: Atomic force microscopy as a multifunctional molecular toolbox in nanobiotechnology. Nat Nanotechnol 3: 261-269, 2008.
23. Samarakoon R and Higgins PJ: MEK/ERK pathway mediates cell-shape-dependent plasminogen activator inhibitor type I gene expression upon drug-induced disruption of the microfilament and microtubule networks. J Cell Sci 115: 3093-3103, 2002.
24. Galluzzi L, Maiuri MC, Vitale I, Zischka H, Castedo M, Zitvogel L and Kroemer G: Cell death modalities: Classification and pathophysiological implications. Cell Death Differ 14: 1237-1243, 2007.
25. Cross SE, Jin YS, Rao J and Gimzewski JK: Nanomechanical analysis of cells from cancer patients. Nat Nanotechnol 2: 780-783, 2007.
26. Nagata S, Hanayama R and Kawane K: Autoimmunity and the clearance of dead cells. Cell 140: 619-630, 2010.
27. Martin SJ, Reutelingsperger CP, McGahon AJ, Rader JA, van Schie RC, LaFace DM and Green DR: Early redistribution of plasma membrane phosphatidylserine is a general feature of apoptosis regardless of the initiating stimulus: Inhibition by overexpression of Bcl-2 and Abl. J Exp Med 182: 1545-1556, 1995.
28. Suzuki J, Denning DP, Imanishi E, Horvitz HR and Nagata S: Xk-related protein 8 and CED-8 promote phosphatidylserine exposure in apoptotic cells. Science 341: 403-406, 2013.
29. Zhang B, Li L, Li Z, Liu Y, Zhang H and Wang J: Carbon ion-irradiated hepatoma cells exhibit coupling interplay between apoptotic signaling and morphological and mechanical remodeling. Sci Rep 6: 35131, 2016.
30. Zhang B, Liu B, Zhang H and Wang J: Erythrocyte stiffness during morphological remodeling induced by carbon ion radiation. PLoS One 9: e112624, 2014.
31. Hessler JA, Budor A, Putchakayala K, Mecke A, Rieger D, Banaszak Holl MM, Orr BG, Bielinska A, Beals J and Baker J Jr: Atomic force microscopy study of early morphological changes during apoptosis. Langmuir 21: 9280-9286, 2005.
32. Gavara N: Combined strategies for optimal detection of the contact point in AFM force-indentation curves obtained on thin samples and adherent cells. Sci Rep 6: 21267, 2016.
33. Sobiepanek A, Milner-Krawczyk M, Lekka M and Kobiela T: AFM and QCM-D as tools for the distinction of melanoma cells with a different metastatic potential. Biosens Bioelectron 93: 274-281, 2017.
34. Zuk A, Targosz-Korecka M and Szymonski M: Effect of selected drugs used in asthma treatment on morphology and elastic properties of red blood cells. Int J Nanomedicine 6: 249-257, 2011.
35. Geiger B, Spatz JP and Bershadsky AD: Environmental sensing through focal adhesions. Nat Rev Mol Cell Biol 10: 21-33, 2009.
36. Magro AM, Magro AD, Cunningham C and Miller MR: Down-regulation of vinculin upon MK886-induced apoptosis in LN18 glioblastoma cells. Neoplasma 54: 517-526, 2007.
37. Elmore S: Apoptosis: A review of programmed cell death. Toxicol Pathol 35: 495-516, 2007.
38. Wu S, Liu X, Zhou X, Liang XM, Gao D, Liu H, Zhao G, Zhang Q and Wu X: Quantification of cell viability and rapid screening anti-cancer drug utilizing nanomechanical fluctuation. Biosens Bioelectron 77: 164-173, 2016.
39. Barros LF, Kanaseki T, Sabirov R, Morishima S, Castro J, Bittner CX, Maeno E, Ando-Akatsuka Y and Okada Y: Apoptotic and necrotic blebs in epithelial cells display similar neck diameters but different kinase dependency. Cell Death Differ 10: 687-697, 2003.
40. Sebbagh M, Renvoizé C, Hamelin J, Riché N, Bertoglio J and Bréard J: Caspase-3-mediated cleavage of ROCK I induces MLC phosphorylation and apoptotic membrane blebbing. Nat Cell Biol 3: 346-352, 2001.
41. Vijayarathna S, Chen Y, Kanwar JR and Sasidharan S: Standardized Polyalthia longifolia leaf extract (PLME) inhibits cell proliferation and promotes apoptosis: The anti-cancer study with various microscopy methods. Biomed Pharmacother 91: 366-377, 2017.
42. Doyle AD and Yamada KM: Cell biology: Sensing tension. Nature 466: 192-193, 2010.
43. Lee B, Leduc PR and Schwartz R: Unified regression model of binding equilibria in crowded environments. Sci Rep 1: 97, 2011.
44. Shew CY, Kondo K and Yoshikawa K: Rigidity of a spherical capsule switches the localization of encapsulated particles between inner and peripheral regions under crowding condition: Simple model on cellular architecture. J Chem Phys 140: 024907, 2014.
45. Humphries JD, Wang P, Streuli C, Geiger B, Humphries MJ and Ballestrem C: Vinculin controls focal adhesion formation by direct interactions with talin and actin. J Cell Biol 179: 1043-1057, 2007.
46. Cui S, Wang J, Wu Q, Qian J, Yang C and Bo P: Genistein inhibits the growth and regulates the migration and invasion abilities of melanoma cells via the FAK/paxillin and MAPK pathways. Oncotarget 8: 21674-21691, 2017.
47. Xu LH, Yang X, Bradham CA, Brenner DA, Baldwin AS Jr, Craven RJ and Cance WG: The focal adhesion kinase suppresses transformation-associated, anchorage-independent apoptosis in human breast cancer cells. Involvement of death receptor-related signaling pathways. J Biol Chem 275: 30597-30604, 2000.

This work is licensed under a Creative Commons Attribution-NonCommercial-NoDerivatives 4.0 International (CC BY-NC-ND 4.0) License.